

Effects of notch structures on DC and RF performances of AlGaN/GaN high electron mobility transistors

Hao Zou(邹浩), Lin-An Yang(杨林安)†, Xiao-Hua Ma(马晓华), and Yue Hao(郝跃)
Citation: Chin. Phys. B, 2021, 30 (**4**): 040502. DOI: 10.1088/1674-1056/abd470
Journal homepage: http://cpb.iphy.ac.cn; http://iopscience.iop.org/cpb

What follows is a list of articles you may be interested in

Influence of sub-bandgap illumination on space charge distribution in CdZnTe detector

Rongrong Guo(郭榕榕, Jinhai Lin(林金海), Lili Liu(刘莉莉), Shiwei Li(李世韦), Chen Wang(王尘), Feibin Xiong(熊飞兵), and Haijun Lin(林海军)
Chin. Phys. B, 2021, 30 (**3**): 036101. DOI: 10.1088/1674-1056/abc67e

CdS/Si nanofilm heterojunctions based on amorphous silicon films: Fabrication, structures, and electrical properties

Yong Li(李勇), Peng-Fei Ji(姬鹏飞), Yue-Li Song(宋月丽), Feng-Qun Zhou(周丰群), Hong-Chun Huang(黄宏春), and Shu-Qing Yuan(袁书卿)
Chin. Phys. B, 2021, 30 (**2**): 026101. DOI: 10.1088/1674-1056/abc15e

Tunable electronic structures of germanane/antimonene van der Waals heterostructures using an external electric field and normal strain

Xing-Yi Tan(谭兴毅), Li-Li Liu(刘利利), Da-Hua Ren(任达华)
Chin. Phys. B, 2020, 29 (**7**): 076102. DOI: 10.1088/1674-1056/ab8a39

Stochastic bifurcations of generalized Duffing-van der Pol system with fractional derivative under colored noise

Wei Li(李伟), Mei-Ting Zhang(张美婷), Jun-Feng Zhao(赵俊锋)
Chin. Phys. B, 2017, 26 (**9**): 090501. DOI: 10.1088/1674-1056/26/9/090501

Modeling the capability of penetrating a jammed crowd to eliminate freezing transition

Mohammed Mahmod Shuaib
Chin. Phys. B, 2016, 25 (**5**): 050501. DOI: 10.1088/1674-1056/25/5/050501

Effects of notch structures on DC and RF performances of AlGaN/GaN high electron mobility transistors*

Hao Zou(邹浩), Lin-An Yang(杨林安)†, Xiao-Hua Ma(马晓华), and Yue Hao(郝跃)

The State Key Discipline Laboratory of Wide Bandgap Semiconductor Technology, School of Microelectronics, Xidian University, Xi'an 710071, *China*

(Received 6 October 2020; revised manuscript received 13 November 2020; accepted manuscript online 17 December 2020)

The effects of various notch structures on direct current (DC) and radio frequency (RF) performances of AlGaN/GaN high electron mobility transistors (HEMTs) are analyzed. The AlGaN/GaN HEMTs, each with a 0.8-μm gate length, 50-μm gate width, and 3-μm source–drain distance in various notch structures at the AlGaN/GaN barrier layer, are manufactured to achieve the desired DC and RF characteristics. The maximum drain current ($I_{ds,max}$), pinch-off voltage (V_{th}), maximum transconductance (g_m), gate voltage swing (GVS), subthreshold current, gate leakage current, pulsed I–V characteristics, breakdown voltage, cut-off frequency (f_T), and maximum oscillation frequency (f_{max}) are investigated. The results show that the double-notch structure HEMT has a 30% improvement of gate voltage swing, a 42.2% improvement of breakdown voltage, and a 9% improvement of cut-off frequency compared with the conventional HEMT. The notch structure also has a good suppression of the current collapse.

Keywords: AlGaN/GaN, high electron mobility transistors (HEMTs), barrier layer, notch

PACS: 05.10.Ln, 61.72.uj, 85.30.Mn, 52.70.Gw **DOI:** 10.1088/1674-1056/abd470

1. Introduction

Due to the superior performances of the high electron mobility transistors (HEMTs) based on AlGaN/GaN heterojunction structure in a wide bandgap, such as high breakdown voltage, high electron velocity, and high current density, they have received a lot of attention in the field of high power and high frequency applications than these HEMTs based on GaAs.[1–6] And many methods have been introduced to improve the high power characteristics, among them the field plate is adopted most.[7–11] There are many types of field plate structures, such as conventional gate field plate,[9,12–14], recessed gate field plate,[15] and Γ-gate with air bridge structure.[16,17] The field plate structure aims to reduce the peak electric field beside the gate electrode, eventually improve the breakdown characteristic. The notch structure in the AlGaN barrier layer proves to reduce the concentration of the two-dimensional electron gas (2DEG) within the channel and also suppress the peak electric field beside the gate electrode.[18–23] The notch structure is achieved by an inductively coupled plasma (ICP) etching system at the AlGaN barrier layer, and the notch structure is parallel to the gate. In this work, the 5 types of notch-structure AlGaN/GaN HEMTs are compared with each other, and their structures to be investigated are named as follows: type-1 referring to the conventional AlGaN/GaN HEMT without a notch structure, type-2 denoting the notch-structure HEMT where the notch is next to the gate and has a depth of 10 nm, type-3 representing the notch-structure HEMT with the notch position being the same as the type-2 but a depth being 15 nm, type-4 being the notch-structure HEMT where the notch is 200 nm away from the gate and has a depth of 10 nm, type-5 signifying the notch-structure HEMT with the notch position being the same as the type-4 but the notch depth being 15 nm, and the type-6 meaning the double-notch structure HEMT where the left notch is 200 nm away from the gate and the right notch is 200 nm away from the left one and they have the same notch depth of 15 nm. Measurements show that the notch-structure HEMTs exhibit superior DC and RF performances compared with the conventional AlGaN/GaN HEMT, and the double-notch structure one exhibits the best performance. Moreover, each of all the AlGaN/GaN HEMTs in this work has an I-gate length of 0.8 μm, aiming to reduce the difficulty in manufacturing and improve the reliability. The manufacturing process of the notch structure at the AlGaN barrier is compatible with the conventional HEMT one.

2. Device structure and manufacture

The AlGaN/GaN heterojunction structure was grown on a 3-in (1 in = 2.54 cm) sapphire substrate, and it was achieved by the metal–organic chemical vapor deposition (MOCVD). The thickness of the GaN buffer layer and the AlGaN barrier layer were 2 μm and 24 nm, respectively. The AlGaN barrier layer was undoped one and the Al composition was 30%. The cross-sectional sizes of the AlGaN/GaN HEMT are shown in Fig. 1.

*Project supported by the National Natural Science Foundation of China (Grant Nos. 61674117 and 61974108) and the State Key Discipline Laboratory of Wide Bandgap Semiconductor Technology of Xidian University, China.

†Corresponding author. E-mail: layang@xidian.edu.cn

© 2021 Chinese Physical Society and IOP Publishing Ltd

AlGaN barrier	24 nm
GaN buffer	2 μm
sapphire substrate	3 in

Fig. 1. Cross-sceional sizes of AlGaN/GaN HEMTs on 3-in sapphire grown by MOCVD.

The electrical properties of the two-dimensional electron gas were measured at room temperature by the Hall measurement, the carrier density was 9.25×10^{12} cm^{-2}, the mobility of the two-dimensional electron gas was 1863 cm^2/(V·s), and the sheet resistance was 361 Ω/sq. In order to have a good comparison among these 6 types of AlGaN/GaN HEMTs, they were fabricated on the same wafer. All these HEMTs had the same cell pitch and device feature size. The distance between the source and drain was 3 μm, the gate was 0.9 μm away from the source, and the width of the device was 50 μm. The length and the depth of the notch structures are denoted as L_n and D_n. The sectional views of these 6 types of AlGaN/GaN HEMTs are shown in Fig. 2.

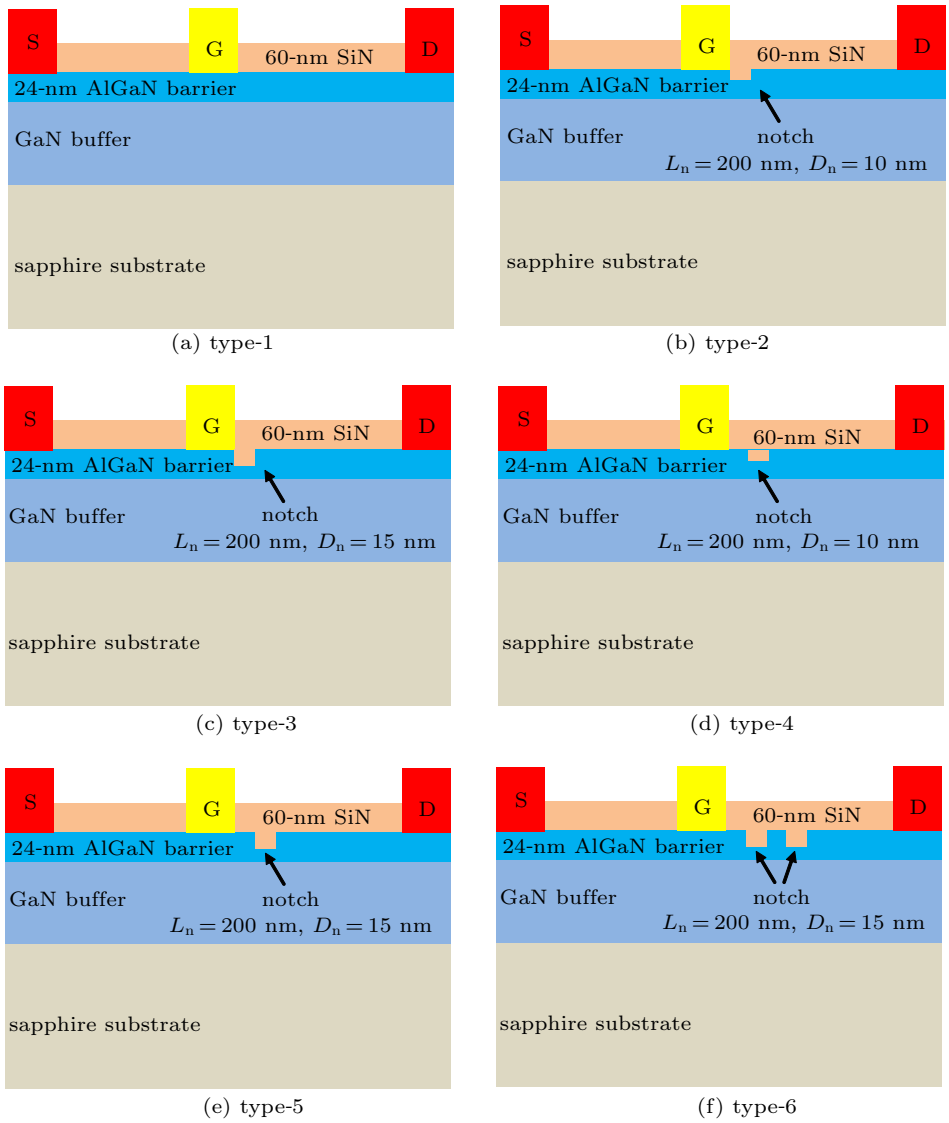


Fig. 2. Schematics of AlGaN/GaN HEMTs with various notch structures.

To fabricate the AlGaN/GaN HEMTs, the manufacturing processes are as follows.

The first step was to preprocess the wafer. The new wafer was soaked in hydrofluoric acid solution ($HF : H_2O = 2 : 3$) for 30 s to remove the surface contaminants. Then the ohmic contact regions of the source and drain electrode were formed by the electron beam evaporation (EBE) and annealed at 880 °C for 30 s in N_2 ambient. The ohmic contact metal was composed of Ti/Al/Ni/Au with the sickness of 20, 160, 55, and 45 nm, respectively. Then the AlGaN/GaN HEMTs were isolated by the mesa etching process, and this step was achieved by the inductively coupled plasma (ICP) etching system based on the Cl_2 and BCl_3, and the mesa height was measured to be 120 nm. The next step was the key step to form the notch struc-

ture. All of the notch regions were defined by an electron beam lithography system (EBL) in the same step. Since the notch structures of the 6 types of HEMTs were in different forms, the manufacturing process of the notch structure has a sequence. In the notch etching process, an ICP etching system based on the Cl_2 and BCl_3 was also adopted, but the etching rate was lower in order to reduce the etching damage. The lower etching rate was obtained by reducing the etching power and the etching gas flow, and the etching depth was controlled by the etching time. Since these proposed notch-structure HEMTs had different depths, in the etching process the Si wafer was used for occlusion. Then a 60-nm SiN passivation layer was deposited on the entire wafer by a plasma-enhanced chemical vapor deposition system (PECVD). In fact, the notch structure was filled with the SiN just like the sectional views shown in Fig. 2. And the SEM images of these 6 types of notch structure are shown in Fig. 3. The next step was to remove the SiN from the source and drain regions so that the ohmic contact regions could be exposed for metal interconnection, and this step still needs an ICP etching system, but it was based on the CF_4 and O_2. And in order to completely remove the SiN passivation layer, a 20% over-etching rate was adopted. Then the gate regions were defined by the stepper, and before the gate metal deposition the ICP based on the CF_4 and O_2 was also used to remove the SiN passivation layer from the gate regions. Then the gate electrode based on the Ni/Au/Ni metal stack was deposited by the electron beam evaporation system (EBE). And the thickness values of the Ni/Au/Ni metal stacks were 45, 200, and 20 nm, respectively. The last step of the manufacturing process was the metal interconnection, which is beneficial to the further test. And the Ti/Au metal stack was also deposited by the electron beam evaporation system (EBE), and the thickness values of the two metals were 20 nm and 200 nm, respectively. The top SEM view of the HEMT is shown in Fig. 4.

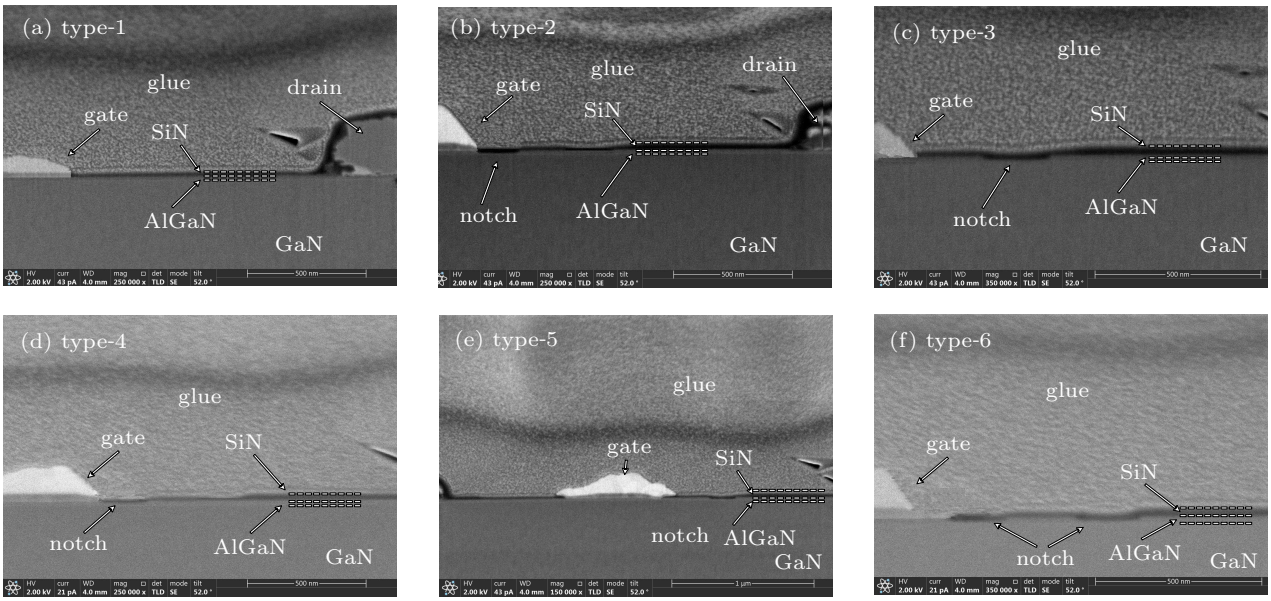


Fig. 3. SEM images of various notch structures.

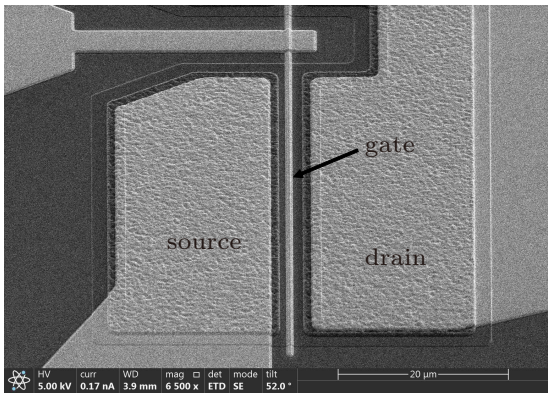


Fig. 4. SEM top view of fabricated AlGaN/GaN high electron mobility transistor (HEMT).

3. Results and discussion

3.1. Simulation results of electric field distribution

The electric field distributions of these 6 types of AlGaN/GaN HEMTs by TCAD simulation are shown in Fig. 5. The simulation size parameters of the HEMTs are the same as those mentioned above. The peak electric field appears at a distance of 1.5 μm from the source. The peak electric fields of the 6 types of HEMTs are 3.1 MV/cm, 2.96 MV/cm, 2.79 MV/cm, 2.80 MV/cm, 2.59 MV/cm, and 2.58 MV/cm. Comparing with the conventional HEMT, the reductions of the notch-structure HEMTs are 4.5%, 10%, 9.7%, 16.5%, and 16.8%, respectively. The conventional HEMT has the highest peak electric field near the gate electrode edge, and the double-

notch structure HEMT has the lowest peak electric field at the same place. The notch structure at the AlGaN barrier layer has a better modulation on the channel electric field because of the closer distance from the channel and the extension of the depletion. Although the notch structure away from the gate at the AlGaN barrier layer causes a lower peak electric field, the notch structure does suppress the peak electric field near the gate electrode edge where the breakdown often happens. Based on the simulation results, the manufacture parameters of the notch structures are determined as mentioned above.

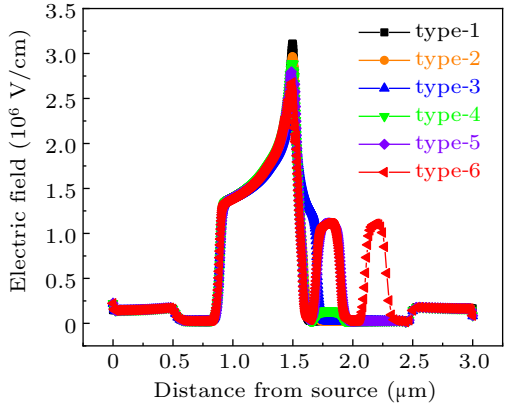


Fig. 5. Electric field distributions of 6 types of AlGaN/GaN HEMTs.

3.2. Transfer characteristics

The measured DC *I*–*V* transfer characteristics of the 6 types of AlGaN/GaN HEMTs are shown in Fig. 6. The gate voltage is from −4 V to 2 V. The threshold voltage is −2.7 V for type-1 HEMT, −2.5 V for type-2 HEMT, −2.2 V for type-3 HEMT, −2.4 V for type-4 HEMT, −2.3 V for type-5 HEMT, and −2.1 V for type-6 HEMT. And their maximum values of drain current ($I_{ds,max}$) are 498.7, 444.8, 415.4, 431.1, 415.9, and 381.2 mA/mm, respectively. The notch structure at the AlGaN barrier layer plays an important role in increasing the channel resistance, resulting in reducing the drain current. The double-notch structure has the maximal increase of resistance and the minimum drain current.

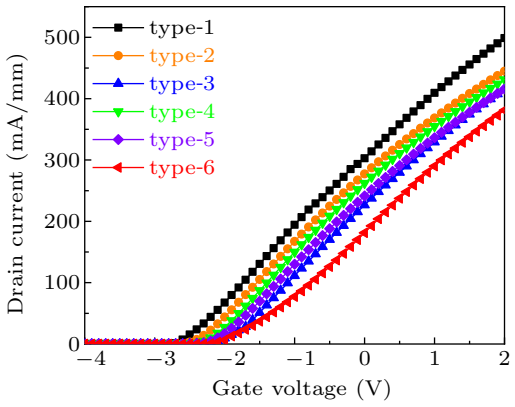


Fig. 6. Transfer characteristics of AlGaN/GaN HEMTs with various notch structures.

The transconductance characteristics of these HEMTs are shown in Fig. 7. The gate voltage is also from −4 V to 2 V. The peak transconductance is 129 mS/mm for type-1 HEMT, 126.9 mS/mm for type-2 HEMT, 121.7 mS/mm for type-3 HEMT, 125.1 mS/mm for type-4 HEMT, 121.3 mS/mm for type-5 HEMT, and 113.7 mS/mm for type-6 HEMT. But the gate voltage swing (GVS) is more important than the peak transconductance in RF application, and the gate voltage swing is defined as the gate voltage range corresponding to a 20% decrease of the peak transconductance. The GVSs of these 6 types of HEMT are 2 V, 2.1 V, 2.4 V, 2.2 V, 2.3 V, and 2.6 V, respectively. The concentration of the 2DEG decreases, which reduces the vertical electrical field near the gate electrode, resulting in a lower peak transconductance. Due to the notch structure at the AlGaN barrier layer, the resistance of the channel increases. When the gate voltage increases, the growth rate of the drain current is limited and not so fast as the case of conventional HEMT. And after the transconductance reaches the saturation region, as the gate voltage increased, the extension of the transconductance decreases.[22,23] The notch-structure HEMTs do have an improvement in the GVS. And the double-notch structure HEMT has a maximum GVS, which is a 30% improvement compared with the conventional HEMT.

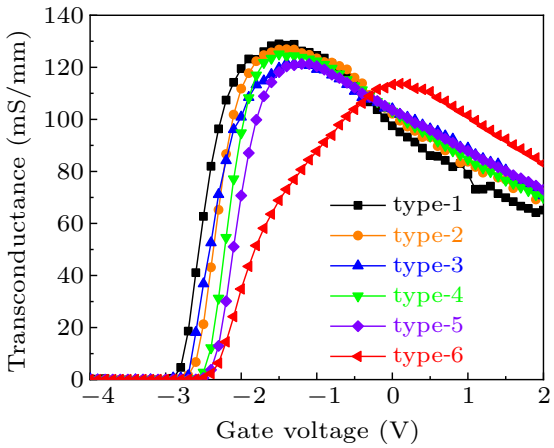


Fig. 7. Transconductance characteristics of AlGaN/GaN HEMTs with various notch structures.

3.3. Leakage current characteristics

The transfer characteristics of the 6 types of HEMTs in logarithmic coordinate system are shown in Fig. 8, when the drain voltage is 6 V. the double-notch structure has the lowest drain current, it also has a close relationship with the resistance in the channel. The subthreshold current and the threshold voltage have the same trend.

The gate leakage current characteristics of these HEMTs are shown in Fig. 9, and the gate voltage ranges from −4 V to 2 V, and the drain voltage is 0 V. The differences in gate leakage current among the 6 types of HEMTs are within an order of magnitude. According to Figs. 8 and 9, we can conclude that the introduction of the notch structure does not cause the surface damage. And the suppression of the peak electrical

field crowding at the gate electrode corner reduces the probability that the electrons are injected into the surface, thus reducing the surface leakage.

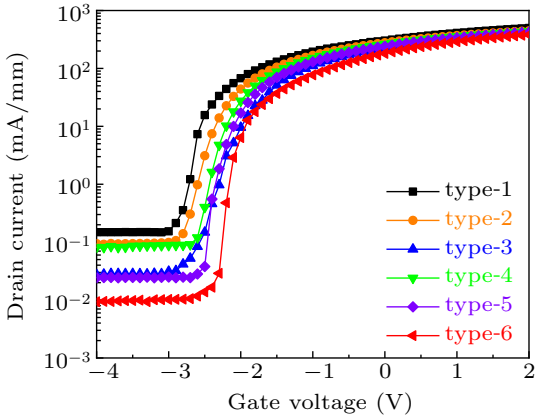


Fig. 8. Transfer characteristics of AlGaN/GaN HEMTs with various notch structures.

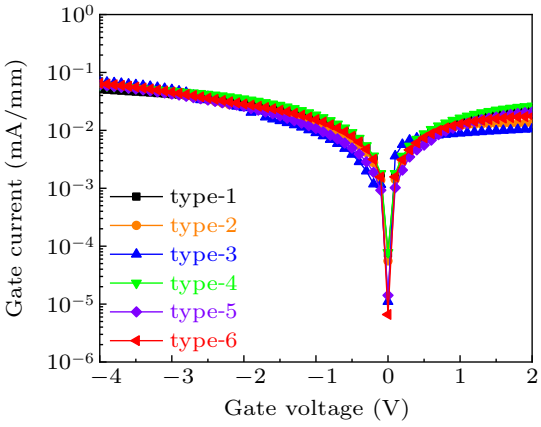


Fig. 9. Gate leakage current characteristics of AlGaN/GaN HEMTs with various notch structures.

3.4. DC characteristics

The output *I*–*V* characteristics of the 6 types of HEMTs are shown in Fig. 10, the gate voltage ranges from −2 V to 2 V and the drain voltage from 0 V to 10 V. Their maximum current densities are 560 mA/mm, 535.7 mA/mm, 491.8 mA/mm, 513 mA/mm, 484.4 mA/mm, and 401.1 mA/mm, respectively.

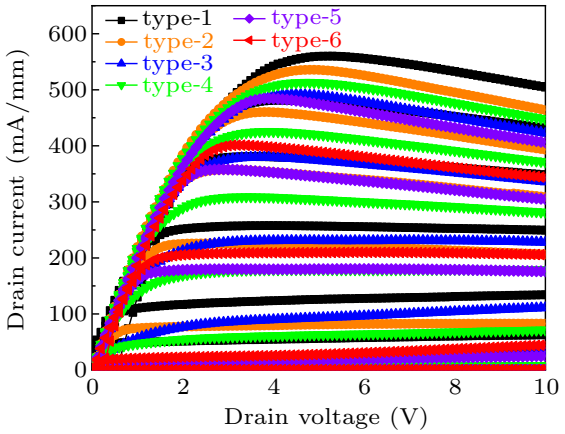


Fig. 10. Output *I*–*V* characteristics of AlGaN/GaN HEMTs with various notch structures.

The pulsed *I*–*V* characteristics of these HEMTs are shown in Fig. 11, the measurement pulse period is 1 ms, and the pulse width is 500 ns. The pulsed *I*–*V* characteristics are tested at the quiescent bias of $(V_{GSQ}, V_{DSQ}) = (0\ V, 0\ V)$ and $(V_{GSQ}, V_{DSQ}) = (-8\ V, 10\ V)$. According to the curves, the maximal reductions of the 6 types of HEMTs are, respectively, 5.2%, 5.0%, 4.0%, 4.5%, 3.9%, and 3.3% when the gate–source voltage is 2 V. The notch structure can suppress the peak electric field, and the decrease of the electric field

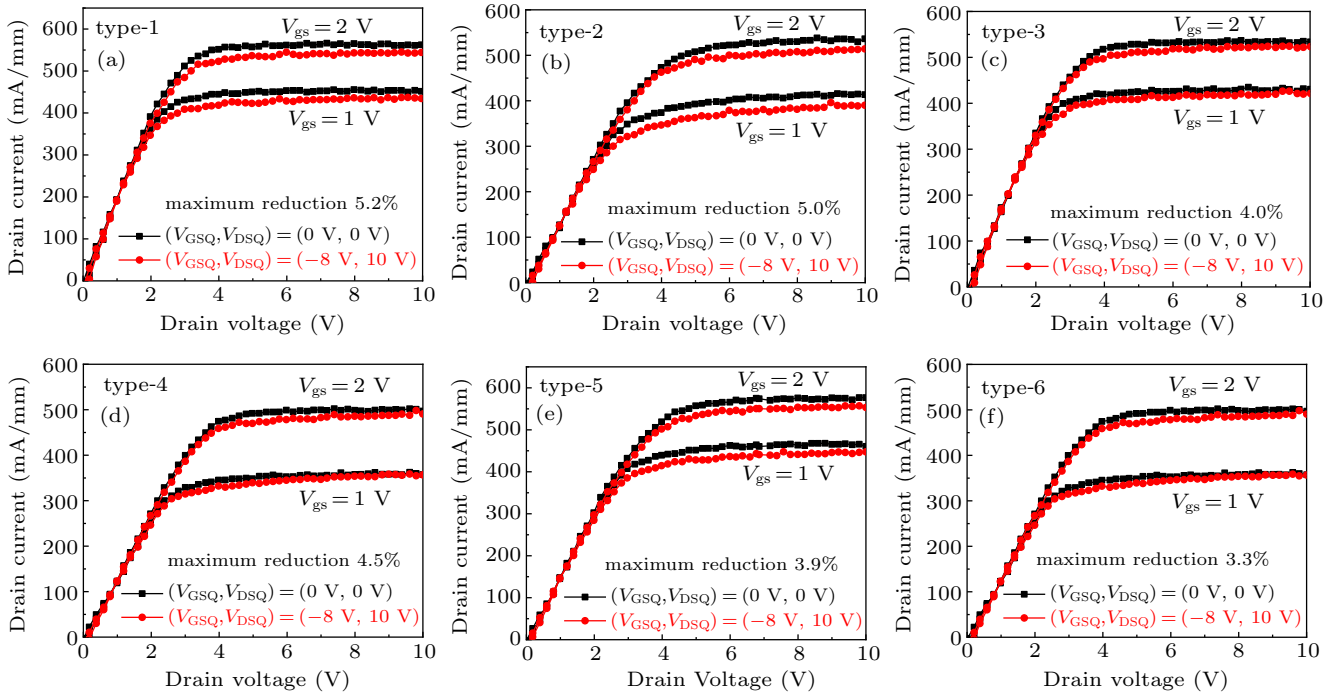


Fig. 11. Pulsed *I*–*V* characteristics of AlGaN/GaN HEMTs with various notch structures.

helps to impede the injection of hot carriers. And the notch structures are filled with the SiN after the passivation process, it can also reduce the surface trapped charge. Thus, the notch-structure HEMTs have a better suppression of the current collapse. It can be concluded that the current collapse is well suppressed for these notch-structure HEMTs.

The breakdown characteristics of the 6 types of HEMTs are shown in Fig. 12, and the gate voltage is set to be −6 V. The off-state breakdown voltage is 71 V for type-1 HEMT, 73 V for type-2 HEMT, 80 V for type-3 HEMT, 77 V for type-4 HEMT, 87 V for type-5 HEMT, and 101 V for type-6 HEMT. The device breakdown often occurs when the electrical field surges at the edge of the gate. The notch structure at the AlGaN barrier layer helps to delay the surge of the electrical field in the channel and impedes the injection of hot carriers. Thus the notch structure improves the breakdown characteristic of the HEMT, and the double-notch HEMT has the highest breakdown voltage of 101 V, which is a 42.2% improvement compared with the conventional HEMT.

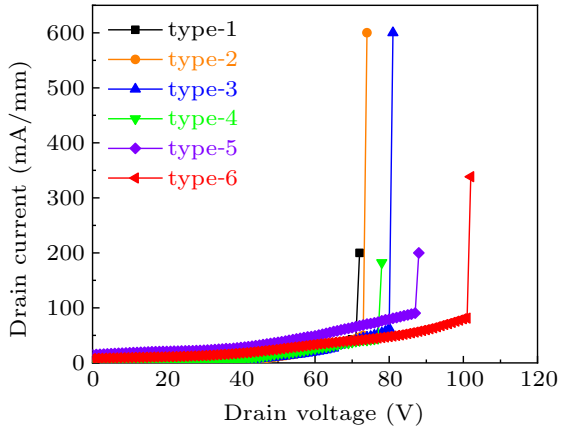


Fig. 12. Breakdown characteristics of AlGaN/GaN HEMTs with various notch structures.

3.5. Small-signal RF characteristics

The small-signal RF characteristics of the 6 types of HEMTs are shown in Figs. 13 and 14. The gate voltage is set to be −1 V, the drain voltage is set to be 3.5 V, and the measurement frequency ranges from 100 MHz to 40 GHz. The current gain (h_{21}) is converted from the *S*-parameters and expressed as

$$h_{21} = \frac{-2S_{21}}{(1-S_{11})(1+S_{22})+S_{12}S_{21}}, \tag{1}$$

where the cut-off frequency (f_T) corresponds to that at $h_{21} =$ 0 dB. The cut-off frequency is 19.3 GHz for type-1 HEMT, 19.5 GHz for type-2 HEMT, 20.1 GHz for type-3 HEMT, 19.6 GHz for type-4 HEMT, 20.2 GHz for type-5 HEMT, and 21.5 GHz for type-6 HEMT. And the values of maximum oscillation frequency f_{max} are 32.3 GHz, 33.6 GHz, 34.6 GHz, 34.3 GHz, 26.2 GHz, and 26.7 GHz for the HEMTs of type-1, type-2, type-3, type-4, type-5, and type-6 respectively. The distance between the gate and the depletion region increases because of the notch structure at the AlGaN barrier layer, and the capacitance between the gate and the drain (C_{gd}) decreases. As a result, the cut-off frequency increases, and the double-notch structure HEMT has a maximum cut-off frequency. But the notch structure makes the resistance in channel increase and the maximum oscillation frequency decrease. Although the double notch structure has a maximum f_T, the f_{max} does not increase as the f_T increases.

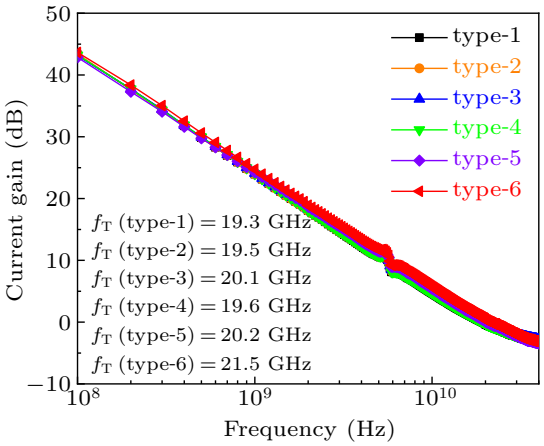


Fig. 13. Current gain characteristics of AlGaN/GaN HEMTs with various notch structures.

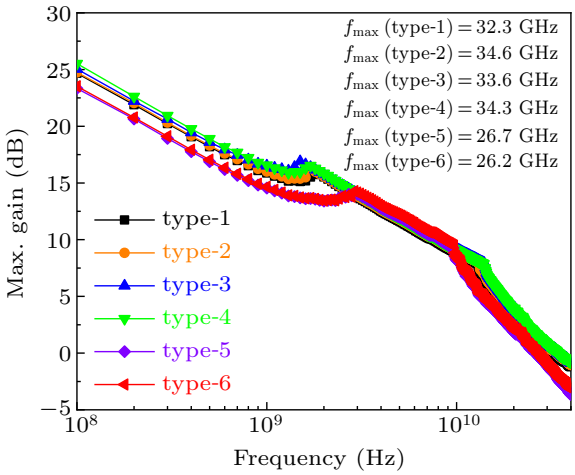


Fig. 14. Maximum oscillation frequency characteristics of AlGaN/GaN HEMTs with various notch structures.

4. Conclusions

The 6 types of AlGaN/GaN HEMTs are investigated and the results are listed in Table 1. Compared with the conventional AlGaN/GaN HEMT, the notch structure at the AlGaN barrier layer improves the DC and RF performances. Especially for the double-notch HEMT, it obtains a 30% improvement of gate voltage swing, a 42.2% improvement of breakdown voltage, and a 9% improvement of cut-off frequency. The notch structure also has a good suppression of the current collapse. All these results indicate that the notch-structure HEMT has potential applications in the areas of high power and high frequency.

Table 1. Results of AlGaN/GaN HEMTs with various notch structures.

Notch structure	Type-1	Type-2	Type-3	Type-4	Type-5	Type-6
$I_{ds,max}$ (mA/mm)	498.7	444.8	415.4	431.1	415.9	381.2
V_{th} (V)	−2.7	−2.5	−2.2	−2.4	−2.3	−2.1
g_m (mS/mm)	129.0	126.9	121.7	125.1	121.3	113.7
GVS (V)	2.0	2.1	2.4	2.2	2.4	2.6
$V_{breakdown}$ (V)	71	73	80	77	87	101
f_T (GHz)	19.3	19.5	20.1	19.6	20.2	21.5
f_{max} (GHz)	32.3	33.6	34.6	34.3	26.2	26.7

References

[1] Mishra U K, Parikh P and Wu Y F 2002 *Proc. IEEE* **90** 1022

[2] Shur M S 1998 *Solid-State Electron* **42** 2131

[3] Saito W, Takada Y, Kuraguchi M, Tsuda K, Omura I, Ogura T and Ohashi H 2003 *IEEE Trans. Electron Dev.* **50** 2528

[4] Mishra U K, Chen L, Kazior T E and Wu Y F 2008 *Proc. IEEE* **96** 287

[5] Roccaforte F, Fiorenza P, Greco G, Nigro R L, Giannazzo F, Lucolano F and Saggio M 2018 *Microelectronic Engineering* **187–188** 66

[6] Ikeda N, Kaya S, Li J, Sato Y, Kato S and Yoshida S 2008 *20th International Symposium on Power Semiconductor Devices and IC's, ISPSD'*08 287–290

[7] Kwak H T, Chang S B, Kim H J, Jang K W, Yoon H, Lee S H, Lim J W and Kim H S 2018 *Appl. Sci.* **8** 974

[8] Kwak H T, Chang S B, Jung H G and Kim H S 2018 *J. Nanosci. Nanotechnol.* **18** 5860

[9] Wu Y F, Saxler A, Moore M, Smith R P, Sheppard S, Chavarkar P M, Wisleder T, Mishra U K and Parikh P 2004 *IEEE Electron Dev. Lett.* **25** 117

[10] Xing H, Dora Y, Chini A, Heikman S, Keller S and Mishra U K 2004 *IEEE Electron Dev. Lett.* **25** 161

[11] Karmalkar S and Mishra U K 2001 *IEEE Trans. Electron Dev.* **48** 1515

[12] Shealy J R, Kaper V, Tilak V, Prunty T, Smart J A, Green B and Eastman L F 2002 *J. Phys.: Condens. Matter* **14** 3499

[13] Kumar V, Chen G, Guo S and Adesida I 2006 *IEEE Trans. Electron Dev.* **53** 1477

[14] Lin C K, Wang W K, Hwu M J and Chan Y J 2004 *J. Vac. Sci. Technol. B* **22** 4

[15] Wang X L, Chen T S, Xiao H L, Wang C M, Hu G X, Luo W J, Tang J, Guo L C and Li J M 2008 *Solid-State Electron.* **52** 926

[16] Palaciosa T, Snow E, Pei Y, Chakraborty A, Keller S, Denbaars S P and Mishra U K 2005 *IEEE International Electron Devices Meeting*, 5 December, 2005, Washington, DC, USA

[17] Pei Y, Poblenz C, Corrion A L, Chu R, Shen L, Speck J S and Mishra U K 2008 *Electron. Lett.* **44** 9

[18] Wang Y, Yang L A, Mao W, Long S and Hao Y 2013 *IEEE Trans. Electron Dev.* **60** 1600

[19] Jia H J, Zhang H, Luo Y H and Yang Z H 2015 *Mater. Sci. Semicond. Process.* **40** 650

[20] Jia H J, Wu Q Y, Luo Y H and Yang Y T 2017 *Superlattices and Microstructures* **111** 841

[21] Razavi S M, Zahiri S H and Hosseini S E 2017 *Pramana J. Phys.* **88** 58

[22] Jia H, Luo Y, Zhang H, Xing D and Ma P M 2017 *Superlattices and Microstructures* **101** 315

[23] Jia H, Zhang H, Luo Y and Yang Z H 2015 *Mater. Sci. Semicond. Process.* **40** 650